Applied Surface Science 479 (2019) 576–581

Contents lists available at ScienceDirect

Applied Surface Science

journal homepage: www.elsevier.com/locate/apsusc

Full length article

Probing the relationship of cations-graphene interaction strength with self-organization behaviors of the anions at the interface between graphene and ionic liquids

Guangliang Hu[a,b,c], Radhika S. Anaredy[d], Mohammed Alamri[c], Qingfeng Liu[c], Gaind P. Pandey[e,f], Chunrui Ma[a,*], Ming Liu[b], Scott K. Shaw[d], Jun Li[e], Judy Z. Wu[c,*]

[a] State Key Laboratory for Mechanical Behavior of Materials, Xi'an Jiaotong University, Xi'an, Shaanxi 710049, China
[b] School of Electronic and Information Engineering, Xi'an Jiaotong University, Xi'an, Shaanxi 710049, China
[c] Department of Physics and Astronomy, University of Kansas, Lawrence, KS 66045, USA
[d] Department of Chemistry, University of Iowa, Iowa City, IA 52242, USA
[e] Department of Chemistry, Kansas State University, Manhattan, KS 66506, USA
[f] Department of Chemistry, Xavier University of Louisiana, New Orleans, LA 70125, USA

ARTICLE INFO

Keywords:
Interfacial layer
Graphene field effect transistor
Ionic liquid
Electrochemical effect

ABSTRACT

The influence of molecular cations on the dynamic self-organization of anion at the interface between graphene and ionic liquid (IL) is investigated by selecting same anion ILs (*N*,*N*-diethyl-*N*-(2-methoxyethyl)-*N*-methylammonium bis(trifluoromethylsulfonyl)imide (DEME-TFSI) and 1-butyl-1-methylpyrrolidinium bis(trifluoromethylsulfonyl)imide (BMP-TFSI)) as the top gate of double-gate graphene filed effect transistors (DG-GFETs). The selected ILs have similar viscosity and conductivity but exhibit distinctly different effects on device performance. From electric transport properties of the DG-GFETs and infrared spectroscopy, it is found that stronger BMP-graphene interactions facilitate faster self-organization of the TFSI anions on graphene. The results introduce an important role of the interfacial cation-graphene interactions that contribute to molecular self-organization, and clearly show the significant impact interfacial effects offer for tuning macroscopic device performance.

1. Introduction

The high thermal and chemical stability, wide electrochemical windows of ionic liquids (ILs) make them a well-established class of materials for organic synthesis, electrolytes in supercapacitors and so on [1–5]. Their properties are closely related to their key functional groups, viscosity, and conductivity. The IL/solid interface has unique molecular architectures, and many prior works contribute to understanding IL properties at a molecular scale [6–9]. The most interesting thing is that the long-range order in IL at the IL/solid interface. However, the ordering of the molecular ions in the ILs is certainly complicated near the IL/solid interface due to complex molecular ions' interaction with each other and with the adjacent solid. In addition, the specific properties of functional groups in ILs can play a critical role in self-ordering of the molecular ions [9]. Thus, understanding molecular interactions and interfacial nuances thereof have significant merit, but requires carefully designed experiments to elucidate the key differences between bulk and interfacial material behaviors.

Double-gate graphene field effect transistors (DG-GFETs) with $Pb_{0.92}La_{0.08}Zr_{0.52}Ti_{0.48}O_3$ (PLZT) back gate and *N*,*N*-diethyl-*N*-(2-methoxyethyl)-*N*-methylammonium bis(trifluoromethylsulfonyl)imide (DEME-TFSI) top gate have been proved an effective way to investigate both static and dynamic behaviors of the interfacial molecule ions in response to external excitations according to our recent work, and we have shown recently that the TSFI anions may self-organize on the graphene surface [10]. This observation sheds light on the mechanism of the electrochemical effect reported as a nonlinear response to the applied electrical field from carbon nanostructure electrodes in electrochemical devices [11–13]. It should be mentioned that molecular ion ordering in the ILs also have been reported by other groups [6,7,9,14–23], and these ordering processes require times of many minutes to hours. Kim et al. reported the ion sizes and molecular structure play an essential role in the interfacial molecular ion layer of IL on graphene that in turn shifts the V_{Dirac} of the graphene [14].

* Corresponding authors.
E-mail addresses: chunrui.ma@mail.xjtu.edu.cn (C. Ma), jwu@ku.edu (J.Z. Wu).

https://doi.org/10.1016/j.apsusc.2019.02.070
Received 20 November 2018; Received in revised form 1 February 2019; Accepted 8 February 2019
Available online 10 February 2019
0169-4332/

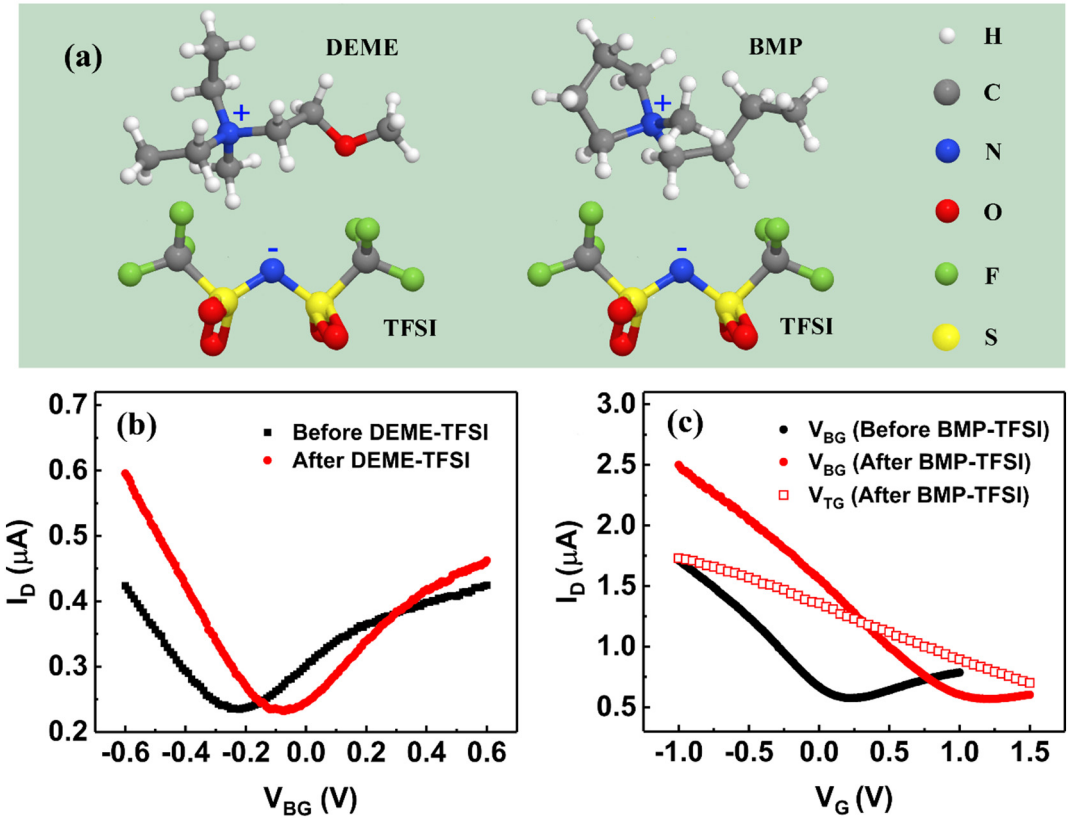

Fig. 1. (a) Molecule structure of DEME-TFSI and BMP-TFSI. (b) and (c) are I_D-V_G curves for DEME-TFSI and BMP-TFSI, respectively.

However, the influence of molecular cations on this self-organization remains unclear. In order uncover this mechanism, we introduce another IL of 1-butyl-1-methylpyrrolidinium bis(trifluoromethylsulfonyl) imide (BMP-TFSI) with the similar viscosity, conductivity and same TFSI anions as DEME-TFSI's [24,25]. However, the DEME and BMP cations have different shapes (Fig. 1a) [26], and chemical interactions. For example, compared to a saturated ring of BMP, the methoxy functional group of the DEME makes it more hydrophilic [27–30].

In this work, a systematic study on the transport properties of the DG-GFETs with DEME-TFSI and BMP-TFSI as top gates was carried out. Importantly, the TFSI interfacial layer effect is observed in devices with both of the ILs. However, we also observed an unexpected and significantly shorter time constant in the self-organization process in the BMP-TFSI case. These results reveal that cations-graphene interactions have important effects on the dynamic self-organization process of TFSI anions, and the resulting electrochemical effect for FET devices.

2. Materials and methods

2.1. Fabrication of epitaxial PLZT film

PLZT thin films of 500 nm thickness on (001) Nb-doped $SrTiO_3$ (Nb:STO) single-crystalline substrates were fabricated by a KrF excimer pulsed laser deposition system with a wavelength 248 nm. The deposition was carried out at an oxygen pressure and temperature of 150 mTorr and 680 °C, respectively. The laser energy density was about 2.0 J cm^{-2} with laser repetition rate of 5 Hz. After the deposition, the PLZT thin films were annealed *in situ* at the growth temperature for 15 min in pure oxygen (350 Torr) before allowing it to cool down to room temperature. The reason for using the PLZT as back gate is both PLZT and ILs are high-efficiency gate with comparable gating efficiencies and a small gate voltage range of ~ ± 1 V, which is adequate to cover the nonlinear electric field range of PLZT without exceeding the electrochemical window of the two ILs used [10,31].

2.2. Ionic liquids

Ionic liquid samples are purchased from IoLiTec (USA) at 99% purity. All ILs are dried under vacuum and stored in a glovebox of < 2 ppm H_2O and < 1 ppm O_2 until use. The viscosity of ILs are measured at 19 °C, both DEME-TFSI and BMP-TFSI exhibit viscosity of ~98 cP. The ILs are visibly clear and show no significant absorptions in the UV–Vis spectral region (Fig. S1). DEME-TFSI and BMP-TFSI exhibit similar capacitance (Fig. S2).

2.3. Graphene fabrication and transfer

Single-layer graphene was grown on commercial polycrystalline copper foils (Sigma-Aldrich, USA) of 25 μm in thickness at ~1000 °C in CH_4/H_2 (4:1) gas mixture in a chemical vapor deposition system [32,33]. In order to transfer the graphene onto the PLZT films, Polymethyl methacrylate (PMMA) was spin-coated on a graphene/Cu sheet and then immersed into copper etchant (CE100) to remove the copper foil. After the copper foil is fully dissolved, the samples were rinsed with deionized (DI) water for multiple times before being transferred onto PLZT thin film to make sure a clean graphene surface is obtained. The PMMA/graphene/PLZT samples were then baked in air at 150 °C for an hour to eliminate moisture. PMMA layer is removed by immersing these samples in acetone followed by isopropyl alcohol rinses and vacuum cleaning to get rid of any residual PMMA left on the graphene surfaces [34,35].

2.4. DG-GFETs fabrication

A similar GFET fabrication process was used in our previous work [31]. The source and drain electrodes were defined on graphene in the

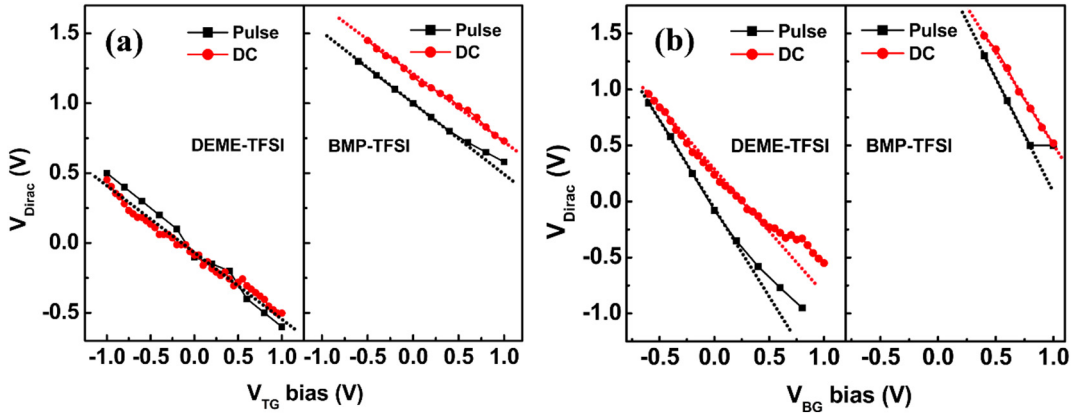

Fig. 2. (a) V_{Dirac}-V_{TG} bias for DC (red) and pulse (black) back gate sweep, (b) V_{Dirac}-V_{BG} bias for DC (red) and pulse (black) top gate sweep for DEME-TFSI DG-GFET and BMP-TFSI DG-GFET.

first photolithography, then, the electrode of 2 nm titanium/88 nm gold was deposited by electron beam evaporation and liftoff. The GFET channel was defined by the second photolithography and the rest of graphene was removed by using oxygen plasma in a reactive ion etcher (RIE, Torr International) at 20 W RF power for 150 s with an oxygen partial pressure of 6.7 mTorr. The graphene channel was 20 (width) × 10 (length) μm^2. Single-layer graphene of the device is evidenced by Raman spectra (Fig. S3). Ionic liquid DEME-TFSI and BMP-TFSI were casted on the GFET channel as the top-gate. The amount of ILs is about 1.5×10^{-5} mL, and the topography of the deposited ILs is microdroplet. The top-gate electric field was applied using a platinum wire (50 μm in diameter) immersed in the ILs. Both of these two ILs have a comparable gating efficiency to that of PLZT [33], which is supported by the similar specific capacitance (~1 to 2 $\mu F/cm^2$ in the frequency range of 1000 to 1 Hz) shown in Fig. S2. This compatibility is critical in operating the DG-GFETs to avoid the gate leakage. In addition, the DEME-TFSI and BMP-TFSI are transparent to visible light [30], allowing perturbation of the electrochemical double layer (EDL) using ultraviolet and visible illumination.

2.5. Characterization

The transport properties of the DG-GFETs were characterized using an Agilent B1500A semiconductor device analyzer in a high-vacuum probe station of $< 2 \times 10^{-6}$ Torr at room temperature. By pumping samples in high vacuum for ~12 h, the complication by water and air may be minimized [34,35]. A broad-band light source (JUNGONG, China) was used for manipulation of the interface molecular ions. The power intensity was calibrated using a Coherent FieldMaxII power meter with OP-2 probe. The infrared reflection absorption spectra (IRRAS) were acquired using a Themo-Nicolet iS50 Fourier transform spectrometer with an external optical bench and liquid-N_2-cooled MCT-A detector. Two sets of samples, one with bare Ag surface and the other with CVD graphene transferred to the Ag surface, were used as substrates to extract the differences in the molecular ion self-organization process on Ag and graphene surfaces. The IL films were made on these two substrates using dynamic wetting technique (described in previous work) [7], which is carried out in an in-house made airtight Polytetrafluoroethylene (PTFE) cell which maintains a controlled gas-phase (dry N_2) environment for the duration of experiments to ensure moisture free atmosphere, and simultaneous *in-situ* probing of the film with infrared radiation in a the reflection geometry.

3. Results and discussion

The schematic of the DG-GFET is shown in Fig. S4. Most measurements, unless otherwise indicated, were performed in a probe station with a base pressure of 5×10^{-6} Torr. The source-drain currents I_D are measured at the varied gate voltage V_G on the DG-GFETs by varying the back-gate voltage (V_{BG}) sweep and top-gate voltage (V_{TG}) sweep from −1.0 V to +1.0 V at a fixed source-drain voltage V_{SD} of 10 mV. The I_D-V_G curves before and after introduce DEME-TFSI and BMP-TFSI were shown in Fig. 1b and c, respectively. It is clearly seen that both Dirac point V_{Dirac} (the potential of minimum conductivity) shifts to right after introduce IL. The right shift indicates that the TFSI anion is absorbed at the graphene/IL interface after introduce ILs and the amount for DEME-TFSI and BMP-TFSI DG-GFET were estimated to be 1.07×10^{12} cm^{-2} and 9.08×10^{12} cm^{-2}, respectively (Supporting Information). According to our previous study, the much more TFSI anion adsorption probably results in stronger electrochemical effect. In order to prove it, the I_D-V_G curves under DC and pulse gate sweeps were performed for both DG-GFETs, which can separate the electrochemical effect and electrostatic effect at the interface [31,34]. The results are shown for these two types of devices respectively in Figs. S5 and S6 with I_D-V_{BG} curves at different fixed V_{TG} biases, and in Figs. S7 and S8 with I_D-V_{TG} curves at different fixed V_{BG} biases. As shown in Figs. S5 and S6, the I_D-V_{BG} curves measured with DC (red) and pulsed (black) V_{BG} sweeps at a given V_{TG} bias follow a similar trend. The V_{Dirac} with the V_{TG} bias are extracted and summarized in Fig. 2a. It can be found the V_{Dirac} in both DEME-TFSI (left) and BMP-TFSI (right) case exhibit a similar linear shift, except a large offset of ~1.0 V on the V_{Dirac} position in the latter case. Considering that the GFET behavior is only affected by the monolayer polar molecules immediately below or above the graphene, this result suggests that the TFSI monolayer pinned on the IL/graphene interface act as an additional static gate field and the applied V_{TG} bias would be simply added on top of the TFSI interfacial gate voltage. It is surprised that there is a minor offset of ~0.28 V between the DC (red) and pulse (black) V_{Dirac} *vs.* V_{TG} curves in the BMP-TFSI case, which is in contrast to the coincided DC and pulse curves in the DEME-TFSI counterparts. The situation becomes much complex when the V_{TG} is used as the sweeping gate with different V_{BG} biases. It is noted that the I_D-V_{TG} curves measured with DC and pulsed V_{TG} sweeps at the positive V_{BG} bias show different trends and only V_{Dirac} under positive V_{BG} were measureable for BMP-TFSI DG-GFET (Figs. S7 and S8). As shown in Fig. 2b, the mismatch of DC and pulse V_{Dirac} for two ILs at positive V_{BG} bias means the electrochemical effect exists in both systems [31]. The relative higher V_{Dirac} under both V_{TG} and V_{BG} bias in BMP-TFSI DG-GFET suggests that the electrochemical effect in BMP-TFSI DG-GFET is stronger than that in DEME-TFSIT DG-GFET.

In order to gain insights on the dynamic behavior of ions at the interface between ILs and graphene for DEME-TFSI and BMP-TFSI, infrared reflection absorption spectra (IRRAS) were taken on two sets of samples. One set has the Ag surface and the other, CVD graphene transferred on Ag substrates. Fig. 3a shows IR data for the ILs deposited

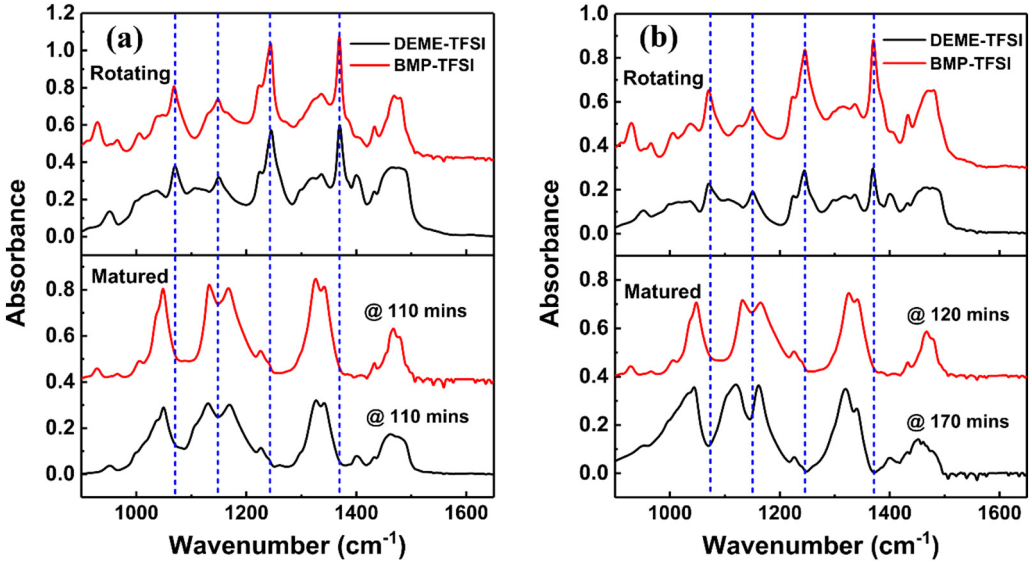

Fig. 3. (a) The top graph shows spectra for freshly prepared DEME-TFSI and BMP-TFSI films on bare silver substrate. Bottom graph compares the same two films after they are completely matured. (b) The same measurement as (a), but the IL films on graphene coated silver substrate.

on the bare Ag substrate (no graphene). The top graph shows spectra for DEME-TFSI and BMP-TFSI films on the bare silver substrate as they are freshly prepared. The bottom graph compares the same two films after they matured (allowed to self-organize) for several tens of minutes. The peaks located at 1069 cm^{-1}, 1149 cm^{-1}, 1244 cm^{-1} and 1366 cm^{-1} after ILs deposition correspond to SNS, SO_2-symmetric, CF_3, and SO_2-asymmetric stretches from the TFSI anion, respectively [7]. The two ILs show similar spectral changes (indicated by vertical dashed lines) as they mature and take the same amount of time to reach maturation (within error ± 10 min), which is in agreement with the linear relationship between maturation time and viscosity reported previously [7]. Both DEME-TFSI and BMP-TFSI exhibit viscosity of ~98 cP at 19 °C. Next, these two ILs are deposited on the graphene substrate and characterized using the same experimental conditions. Results are shown in Fig. 3b. Comparing the two ILs in the lower frequency region below 1400 cm^{-1}, which is characteristic of the TFSI anion, it can be seen that the two ILs show very similar spectral features at their maturation times. However, the maturation times are not the same on graphene. Specifically, 120 min is required for BMP-TFSI, which is considerably shorter than the 170 min required for DEME-TFSI. Considering the principle variable between the two ILs is the cations (DEME *vs* BMP) and the discrepancy in the maturation time in spite of same viscosity is observed only on the graphene samples, the difference in the strength of the interaction between the IL and graphene surface could be a reasonable origin.

In order to probe the strength of the interaction, an ultraviolet-visible light (emission spectrum shown in Fig. S9) was introduced to nondestructively activate and de-organize the formed TFSI molecular anion monolayer while monitoring I_D-V_G characteristic during and after the illumination. The probe station was maintained at ~1 Torr for about 12 h before backfilling to about 720 Torr with dry N_2 to exclude influence of water or other airborne species. This simulated environment without water, and at atmospheric pressure, is similar to the conditions used for infrared spectroscopy. The I_D-V_{BG} curves taken at selected time points before and after the illumination are shown in Fig. S10a and b for DEME-TFSI and BMP-TFSI DG-GFETs, respectively. The changes of V_{Dirac} are picked up and shown in Fig. 4a. 60 mW/cm^2 was applied in both cases. Quantitative differences exist between the two cases. For example, with 60 min of light illumination, the V_{Dirac} of the DEME-TFSI DG-GFETs can be shifted to almost zero volts (~0.08 V) while V_{Dirac} reaches only ~0.32 V in the case of the BMP-TFSI DG-GFETs. Considering the two ILs are on the GFETs of similar surfaces, the slower shift of the V_{Dirac} may be attributed to a stronger TFSI organization activities in the latter. This argument seems consistent with the faster recovering rates for ordered interfacial TFSI layer after the light was turned off (Fig. 4b). Fig. 4b shows the comparison of V_{Dirac} changes between DEME-TFSI and BMP-TFSI DG-GFETs at selected times after the light (60 mW/cm^2 for 40 min) was turned off, the details of I_D-V_{BG} characteristics are shown in Fig. S10c and d. This data shows that, after the light was off for 5 min, the shift of V_{Dirac} of BMP-TFSI DG-GFET (~0.22 V) is larger than that of DEME-TFSI DG-GFET (~0.12 V). This further indicates that the TFSI ions in BMP-TFSI that are disordered by illumination can quickly return to the interface, likely due to a stronger interaction between the BMP and graphene. In order to confirm it, we consider to apply a positive top gate voltage (+1 V) to both DG-GFET after light illumination for long time, since the applied voltage will make the randomly ions to arrange orderly. That is, the BMP and DEME cations will move to graphene, as shown in Fig. 5a (V_{TG} = +1 V). Then, we remove the positive top gate voltage, the cations will depart from graphene (Fig. 5a, V_{TG} = 0 V, after V_{TG} = +1 V). The departure rate is determined by the interaction strength between cations and graphene. The stronger interaction strength, the departure rate will be lower, which result in different V_{Dirac}. Fig. 5b and c compares the I_D-V_{BG} characteristics measured after the light illumination for 40 mins on both DEME-TFSI and BMP-TFSI DG-GFETs, respectively. In both figures, the black curve was measured at V_{TG} = 0 V, red curve was measured after V_{TG} was set to +1.0 V (the EDL on graphene will make positive ions toward graphene as the schematic picture Fig. 5a (V_{TG} = +1 V) and then back to 0 V. On the DEME-TFSI DG-GFETs, the black and red curves coincide well in Fig. 5b. This, however, does not happen in BMP-TFSI DG-GFETs case. As shown in Fig. 5c, the V_{Dirac} shifts from 0.48 V (V_{TG} = 0 V) to 0.71 V (V_{TG} to +1 V, then to 0 V). These results indicate that the interaction between DEME cations and graphene is so weak that they can escape from graphene easier and recover to its original position. Unlike DEME cations, the interaction between BMP cations and graphene is strong, which induce extra BMP cations left near the graphene even the applied top-gate voltage is removed. The positive shift in BMP-TFSI case is due to the extra BMP cations attracts more TFSI anions and the bigger mass TFSI prefer toward graphene, according to Kim et al. report that when the mass of cation is smaller than that of anion, the V_{Dirac} shifts to positive side, while in the opposite case the V_{Dirac} shifts to negative side [14].

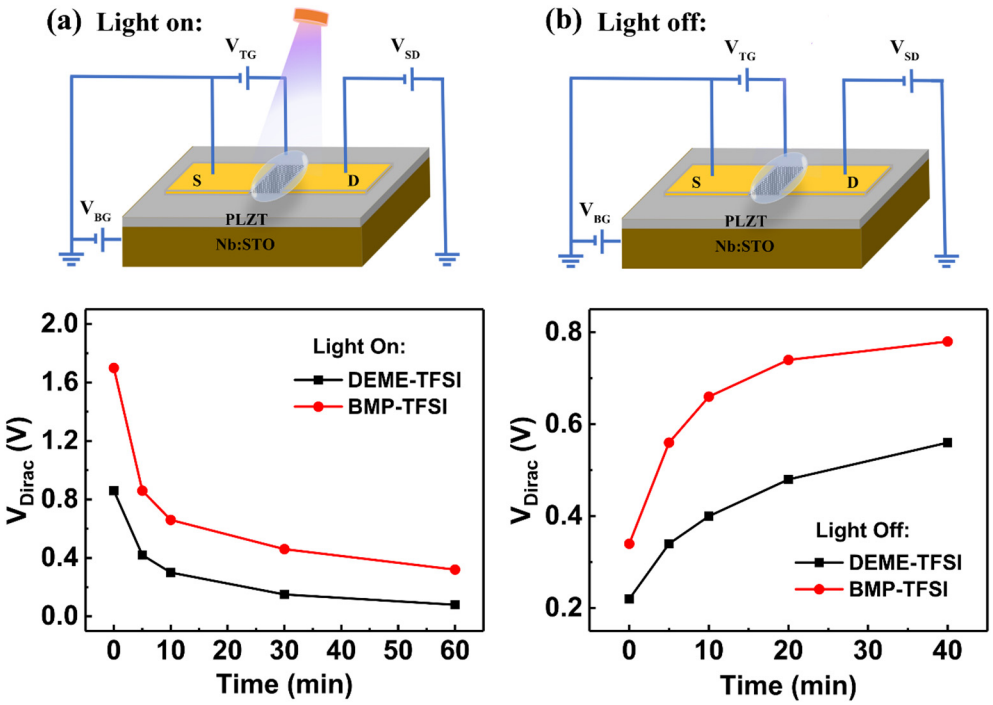

Fig. 4. (a) The V_{Dirac} with time going (down) for DEME-TFSI (black) and BMP-TFSI (red) DG-GFETs taken at selected times after the light with 60 mW/cm^2 was turned on (up). (b) The V_{Dirac} with time going (down) for DEME-TFSI (black) and BMP-TFSI (red) DG-GFETs taken at selected times after the light illumination for 40 mins and was turned off (up).

4. Conclusions

In this work, DEME-TFSI and BMP-TFSI ionic liquids, they are commonly used in a large variety of electrochemical and opto-electrochemical devices with unique solubility characteristics, good ionic conductivity, low viscosity and thermally, electrochemically stable in a wide potential window [36,37], are employed as the top gates of the DG-GFETs. In both DEME-TFSI and BMP-TFSI, our data indicate formation of an ordered interfacial molecular anion layer at the IL/graphene interface. Considering the two ILs have comparable viscosity and

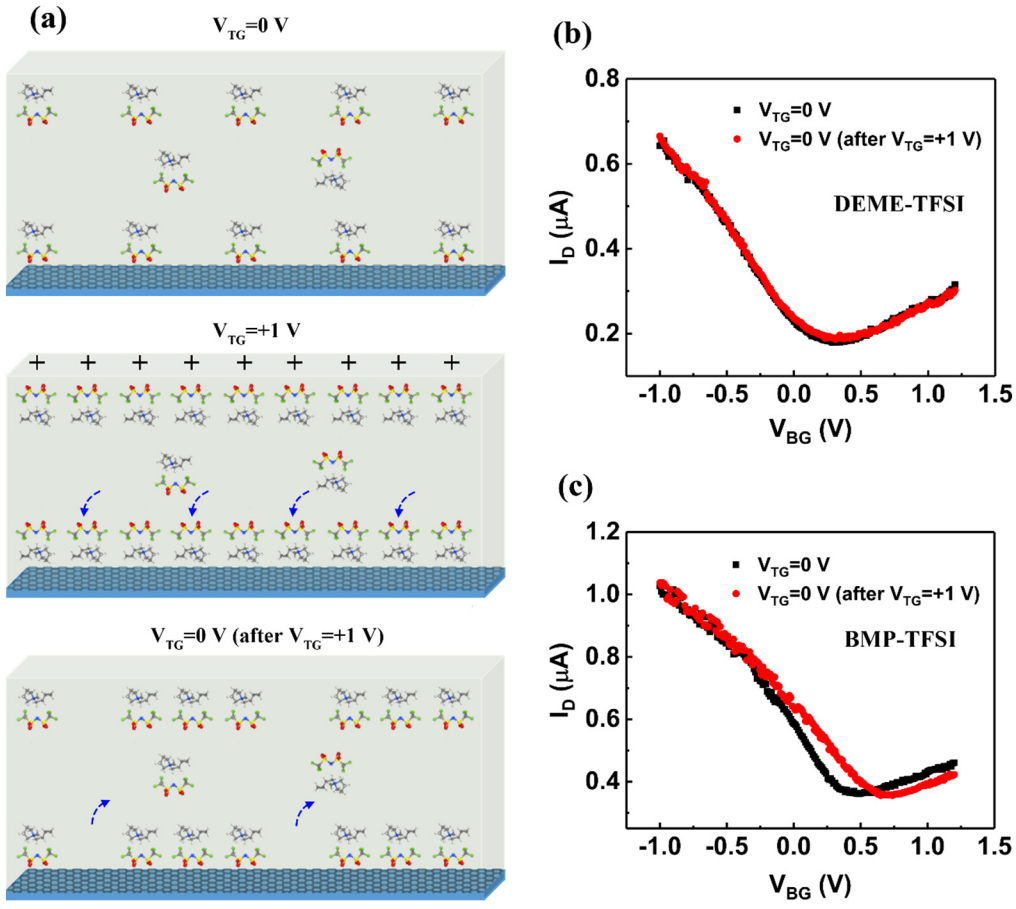

Fig. 5. (a) Schematic of the dynamic interaction between graphene and molecular ions in ionic liquids response to the electric field. I_D-V_{BG} characteristic measured on: (b) DEME-TFSI and (c) BMP-TFSI gated DG-GFETs at V_{TG} = 0 V (black) and after V_{TG} was set to +1.0 V and then back to 0 V (red) after 40 mins of light illumination at 60 mW/cm^2.

bulk conductivity, the DEME-TFSI and BMP-TFSI gated DG-GFETs provide a unique platform to extract specific cation effects on the dynamic self-organization process. Based on the different dynamic process of self-organization as well as de-organization behavior under light activation of the interfacial molecular TFSI layer in these two DG-GFETs, we propose that the differences primarily result from the cation interaction with graphene and a stronger cation-graphene interaction leads to formation of a stronger self-organized TFSI layer and a weaker de-organization of anion through photo-response and electric-response data of DG-GFETs. The dynamic information provided in this study are helpful to understand general IL behavior in application environments and clearly convey the importance of substrate-ion or cation-anion interactions when predicting performance, especially for systems of apparently similar physicochemical properties. These results reveal rich dynamics of IL ion interactions with graphene and reinforce the importance of material dynamics in device performance.

Acknowledgments

The authors acknowledge support in part by the Fundamental Research Funds for the Central Universities, NASA contract NNX13AD42A, ARO contract W911NF-16-1-0029, and NSF contract NSF-DMR-1337737 and NSF-DMR1508494. This research also was supported by Natural Science Foundation of China No. 51390472 and 51702255, National “973” projects of China (No.2015CB654903), China Postdoctoral Science Foundation No. 2015M582649, NSFC-NGC 61631166004. SKS acknowledges funding from NSF award 1651381, ACS Petroleum Research Fund award 55279-DNI5, and the Research Corporation for Science Advancement's Cottrell Scholar award funding.

Appendix A. Supplementary data

Supplementary data to this article can be found online at https://doi.org/10.1016/j.apsusc.2019.02.070.

References

[1] R.D. Rogers, K.R. Seddon, Ionic liquids - solvents of the future? Science 302 (2003) 792–793.
[2] C. Arbizzani, M. Biso, D. Cericola, M. Lazzari, F. Soavi, M. Mastragostino, Safe, high-energy supercapacitors based on solvent-free ionic liquid electrolytes, J. Power Sources 185 (2008) 1575–1579.
[3] Shalu, V.K. Singh, R.K. Singh, Development of ion conducting polymer gel electrolyte membranes based on polymer PVdF-HFP, BMIMTFSI ionic liquid and the Li-salt with improved electrical, thermal and structural properties, J. Mater. Chem. C 3 (2015) 7305–7318.
[4] M. Singh, K. Manoli, A. Tiwari, T. Ligonzo, C. Di Franco, N. Cioffi, G. Palazzo, G. Scamarcio, L. Torsi, The double layer capacitance of ionic liquids for electrolyte gating of ZnO thin film transistors and effect of gate electrodes, J. Mater. Chem. C 5 (2017) 3509–3518.
[5] A.B. Chen, Y.Q. Li, L. Liu, Y.F. Yu, K.C. Xia, Y.Y. Wang, S.H. Li, Controllable synthesis of nitrogen-doped hollow mesoporous carbon spheres using ionic liquids as template for supercapacitors, Appl. Surf. Sci. 393 (2017) 151–158.
[6] K. Ma, R. Jarosova, G.M. Swain, G.J. Blanchard, Charge-induced long-range order in a room-temperature ionic liquid, Langmuir 32 (2016) 9507–9512.
[7] R.S. Anaredy, S.K. Shaw, Long-range ordering of ionic liquid fluid films, Langmuir 32 (2016) 5147–5154.
[8] R.S. Anaredy, A.J. Lucio, S.K. Shaw, Adventitious water sorption in a hydrophilic and a hydrophobic ionic liquid: analysis and implications, ACS Omega 1 (2016) 407–416.
[9] S.Y. Xu, S.R. Xing, S.S. Pei, V. Ivanistsev, R. Lynden-Bell, S. Baldelli, Molecular response of 1-butyl-3-methylimidazolium dicyanamide ionic liquid at the graphene electrode interface investigated by sum frequency generation spectroscopy and molecular dynamics simulations, J. Phys. Chem. C 119 (2015) 26009–26019.
[10] G.L. Hu, G.P. Pandey, Q.F. Liu, R.S. Anaredy, C.R. Ma, M. Liu, J. Li, S.K. Shaw, J. Wu, Self-organization of ions at the interface between graphene and ionic liquid DEME-TFSI, ACS Appl. Mater. Interfaces 9 (2017) 35437–35443.
[11] G.K. Veerasubramani, K. Krishnamoorthy, P. Pazhamalai, S.J. Kim, Enhanced electrochemical performances of graphene based solid-state flexible cable type supercapacitor using redox mediated polymer gel electrolyte, Carbon 105 (2016) 638–648.
[12] M. Shi, S. Kou, X. Yan, Engineering the electrochemical capacitive properties of graphene sheets in ionic-liquid electrolytes by correct selection of anions, ChemSusChem 7 (2014) 3053–3062.
[13] A. Prakash, D. Bahadur, The role of ionic electrolytes on capacitive performance of ZnO-reduced graphene oxide nanohybrids with thermally tunable morphologies, ACS Appl. Mater. Interfaces 6 (2014) 1394–1405.
[14] U.J. Kim, T.G. Kim, Y. Shim, Y. Park, C.W. Lee, T.H. Kim, H.S. Lee, D.Y. Chung, J. Kihm, Y.G. Roh, J. Lee, H. Son, S. Kim, J. Hur, S.W. Hwang, Modulation of the dirac point voltage of graphene by ion-gel dielectrics and its application to soft electronic devices, ACS Nano 9 (2015) 602–611.
[15] M.Q. Chu, M. Miller, T. Douglas, P. Dutta, Ultraslow dynamics at a charged silicon-ionic liquid interface revealed by X-ray reflectivity, J. Phys. Chem. C 121 (2017) 3841–3845.
[16] S.Y. Xu, S.R. Xing, S.S. Pei, S. Baldelli, Sum frequency generation spectroscopy study of an ionic liquid at a graphene-BaF_2 (111) Interface, J. Phys. Chem. B 118 (2014) 5203–5210.
[17] M.A. Devanathan, B.V. Tilaik, The structure of the electrical double layer at the metal-solution interface, Chem. Rev. 65 (1965) 635–684.
[18] S.A. Kislenko, I.S. Samoylov, R.H. Amirov, Molecular dynamics simulation of the electrochemical interface between a graphite surface and the ionic liquid [BMIM][PF6], Phys. Chem. Chem. Phys. 11 (2009) 5584–5590.
[19] O. Höfft, S. Bahr, V. Kempter, Investigations with infrared ipectroscopy on films of the ionic liquid [EMIM]Tf2N, Langmuir 24 (2008) 11562–11566.
[20] J. Luczak, J. Hupka, J. Thoming, C. Jungnickel, Self-organization of imidazolium ionic liquids in aqueous solution, Colloids Surf. A Physicochem. Eng. Asp. 329 (2008) 125–133.
[21] J.C.S. Costa, A.F.S.M.G. Coelho, A. Mendes, L.M.N.B.F. Santos, Nucleation and growth of microdroplets of ionic liquids deposited by physical vapor method onto different surfaces, Appl. Surf. Sci. 428 (2018) 242–249.
[22] J.N.A.C. Lopes, A.A.H. Padua, Nanostructural organization in ionic liquids, J. Phys. Chem. B 110 (2006) 3330–3335.
[23] W. Jiang, Y.T. Wang, G.A. Voth, Molecular dynamics simulation of nanostructural organization in ionic liquid/water mixtures, J. Phys. Chem. B 111 (2007) 4812–4818.
[24] S. Zhang, N. Sun, X. He, X. Lu, X. Zhang, Physical properties of ionic liquids: database and evaluation, J. Phys. Chem. Ref. Data 35 (2006) 1475–1517.
[25] U. Ulissi, A. Elia Giuseppe, S. Jeong, F. Mueller, J. Reiter, N. Tsiouvaras, Y.K. Sun, B. Scrosati, S. Passerini, J. Hassoun, Low-polarization lithium–oxygen battery using [DEME][TFSI] ionic liquid electrolyte, ChemSusChem 11 (2017) 229–236.
[26] L. Chen, S.F. Zhao, Y.P. Liu, M. Horne, A.M. Bond, J. Zhang, Room temperature electrodeposition of metallic magnesium from ethylmagnesium bromide in tetrahydrofuran and ionic liquid mixtures, J. Electrochem. Soc. 163 (2016) H3043–H3051.
[27] S. Sankarasubramanian, J. Seo, F. Mizuno, N. Singh, K. Takechi, J. Prakash, Enhancement of oxygen reduction reaction rate by addition of water to an oxidatively stable ionic liquid electrolyte for lithium-air cells, Electrochem. Commun. 73 (2016) 55–58.
[28] F. Wohde, M. Balabajew, B. Roling, Li+ transference numbers in liquid electrolytes obtained by very-low-frequency impedance spectroscopy at variable electrode distances, J. Electrochem. Soc. 163 (2016) A714–A721.
[29] N. Wongittharom, C.H. Wang, Y.C. Wang, C.H. Yang, J.K. Chang, Ionic liquid electrolytes with various sodium solutes for rechargeable Na/$NaFePO_4$ batteries operated at elevated temperatures, ACS Appl. Mater. Interfaces 6 (2014) 17564–17570.
[30] G.W. Xu, R.T. Lu, J.W. Liu, H.Y. Chiu, R.Q. Hui, J.Z. Wu, Photodetection based on ionic liquid gated plasmonic Ag nanoparticle/graphene nanohybrid field effect transistors, Adv. Opt. Mater. 2 (2014) 729–736.
[31] C. Ma, R. Lu, G. Hu, J. Han, M. Liu, J. Li, J. Wu, Detecting electric dipoles interaction at the interface of eerroelectric and electrolyte using graphene field effect transistors, ACS Appl. Mater. Interfaces 9 (2017) 4244–4252.
[32] Q.F. Liu, Y.P. Gong, J.S. Wilt, R. Sakidja, J. Wu, Synchronous growth of AB-stacked bilayer graphene on Cu by simply controlling hydrogen pressure in CVD process, Carbon 93 (2015) 199–206.
[33] J.T. Ye, S. Inoue, K. Kobayashi, Y. Kasahara, H.T. Yuan, H. Shimotani, Y. Iwasa, Liquid-gated interface superconductivity on an atomically flat film, Nat. Mater. 9 (2010) 125–128.
[34] C. Ma, Y. Gong, R. Lu, E. Brown, B. Ma, J. Li, J. Wu, Detangling extrinsic and intrinsic hysteresis for detecting dynamic switch of electric dipoles using graphene field-effect transistors on ferroelectric gates, Nanoscale 7 (2015) 18489–18497.
[35] R.T. Lu, J.W. Liu, H.F. Luo, V. Chikan, J.Z. Wu, Graphene/GaSe-nanosheet hybrid: towards high gain and fast photoresponse, Sci. Rep. 6 (2016) 19161.
[36] S.D. Talian, M. Bester-Rogac, R. Dominko, The physicochemical properties of a [DEME][TFSI] ionic liquid-based electrolyte and their influence on the performance of lithium-sulfur batteries, Electrochim. Acta 252 (2017) 147–153.
[37] J.X. Mao, H.B. Nulwala, D.R. Luebke, K. Damodaran, Spectroscopic and computational analysis of the molecular interactions in the ionic liquid ion pair [BMP](+)[TFSI](−), J. Mol. Liq. 175 (2012) 141–147.